https://doi.org/10.5194/egusphere-2026-5405
Preprint. Discussion started: 21 September 2026

CO_2 exchange at a subarctic mire complex with varying permafrost status

Patryk Łakomiec[1,2], Jutta Holst[2], Niklas Rakos[3], Erik Lundin[3], Patrick Crill[4], Thomas Friborg[5], Hongxiao Jin[2], Lars Eklundh[2], Janne Rinne[6]

[1]FAAM Airborne Laboratory, National Centre for Atmospheric Science, MK43 0AL, Cranfield, UK,

[2]Department of Earth and Environmental Sciences, Lund University, 223 62, Lund, Sweden

[3]Abisko Scientific Research Station, Swedish Polar Research Secretariat, 981 07, Abisko, Sweden

[4]Department of Geological Sciences and Bolin Centre for Climate Research, Stockholm University, 114 19, Stockholm, Sweden

[5]Department of Geosciences and Natural Resource Management, University of Copenhagen, 1165, Copenhagen, Denmark

[6]Natural Resources Institute Finland (Luke), 00790, Helsinki, Finland

Correspondence to: Patryk Łakomiec (patlakomiec@gmail.com)

Abstract

Thawing permafrost exerts a major forcing on carbon cycling in peatlands along the margins of the Arctic. Our aim in this work is to quantify the differences in net ecosystem exchange (NEE) of CO_2 and its component processes — Gross Primary Production (GPP) and ecosystem respiration (Reco) — across surfaces with different permafrost status in a sub-arctic mire complex. The study site, the Abisko-Stordalen mire in Arctic Sweden, is located at 68°20' N, 19°30' E. We used data from two eddy covariance towers, with footprints covering areas with different permafrost status, i.e. mostly permafrost covered palsa plateau (2014-2021), partly thawed bog-palsa mosaic (2014-2021), and non-permafrost rich fen (2014). The bi-modal wind direction pattern at the measurement site helped to derive surface type specific data data set from each tower.

The diel cycle of carbon dioxide (CO_2) fluxes during the summer months (June, July, and August) were similar in their pattern, but the magnitudes of CO_2 fluxes at the fen exhibited higher fluxes than the palsa and thawing sectors. The CO_2 fluxes between the palsa plateau and partly thawed area were like each other. CO_2 responses to air temperature and incoming solar radiation indicated highest Reco and GPP and any given temperature and light level at the non-permafrost fen.

Analysis of the gapfilled NEE at the palsa plateau and partially thawed sector, for which multi-year time series is available, showed that 2016 had significantly higher fluxes than the multi-year average. The likely reason for this is the longer growing season in 2016. This is also supported by the locally measured NDVI values, suggesting greater vegetation development during that year.

https://doi.org/10.5194/egusphere-2026-5405
Preprint. Discussion started: 21 September 2026

In summary, the tall sedge fen had the highest daytime CO_2 uptake in summer and the highest net respiration at night during the growing season. The palsa plateau and partially thawed sector exhibited significantly lower CO_2 fluxes. There were no significant differences in NEE, GPP, or Reco between these two sectors, despite their differing permafrost conditions and vegetation characteristics. This is in contrast with significant differences in methane emissions between these three systems reported in previous studies.

1. Introduction

In recent years, the high latitudes have experienced more pronounced warming in comparison to lower latitudes (Post et al., 2019). This swift warming trend is anticipated to endure into the forthcoming years (Serreze et al., 2011; Biskaborn et al., 2019). The increase in temperature is expected to accelerate the thawing of permafrost, leading to amplified microbial decomposition rates and heightened temperature sensitivity of the soil carbon stability (Schuur et al., 2008; Koven et al., 2017). Consequently, permafrost soil carbon is becoming increasingly vulnerable to depletion (Crowther and Bradford, 2013; MacDougall et al., 2016; Burke et al., 2017; Varney et al., 2020; Wilson et al. 2022) and release of remineralizer carbon to atmospheric carbon dioxide (CO_2). The geographical features of the Arctic can be transformed due to the thawing of permafrost and thermokarst formation, resulting in the collapse of soil structures, redistribution of the near surface water tables, and the creation of open water reservoirs (Åkerman and Johansson, 2008). The surface water in thawing permafrost mire is determined by the microtopography and permafrost dynamics, which has impact on the composition of plant communities and the oxidative status of mire soils. That transformation will lead to changes in the wetlands type, from palsa and bog to fen and open water (Varner et al., 2022) and changes in ground temperatures, active layer thickness, plant community structure, and productivity (Johansson et al., 2013). Carbon gas budgets for the northern permafrost region are still uncertain due to low data availability (Ramage et al. 2024). Lack of temporal and spatial information on fluxes of climate forcing gases, or greenhouse gases (GHG), in this heterogeneous landscape causes uncertainty in global budget estimations (Watts et al., 2023). Changes in terrestrial temperature at high latitudes reveal significant amounts of organic carbon (OC), consequently leading to the degradation of C and the emission of GHGs such as CO_2 and methane (CH_4) from permafrost into the atmosphere (Chen et al., 2021; Natali et al., 2019; Schuur et al., 2009, 2015; Treat et al., 2018; Voigt et al., 2020a). Higher annual air temperatures make the growing season longer. This is leading to increase in CO_2 fluxes and additional nutrient release from thawing permafrost. This may contribute to increased vegetation productivity that at least partly offset the release of permafrost GHG. (Koven et al., 2015; Liu, Kuhn, et al., 2022; López-Blanco et al., 2022; McGuire et al., 2018; Schuur & Mack, 2018).

The main goal of this work is to quantify the differences in net ecosystem exchange of CO_2 (NEE) and its component processes, Gross Primary Production (GPP) and ecosystem respiration (Reco), across mire surfaces with different permafrost status at a sub-arctic mire complex using eddy covariance (EC) data. The EC method is suitable for long-term, high temporal resolution

https://doi.org/10.5194/egusphere-2026-5405
Preprint. Discussion started: 21 September 2026

measurements (e.g Knox et al., 2016; Li et al., 2016, Rinne et al. 2018) with minimal disturbance to the measured surface. Multi-year observations allow for the identification of patterns, annual and interannual variation in CO_2 exchange. Datasets spanning over extended periods of time are crucial for comprehending the dynamics of ecosystems, evaluating the effects of climate change, and guiding policy-making processes.

This study encompasses CO_2 fluxes of three different areas measured by two EC system. Previously the C fluxes at these surface types have been compared by chamber (Bäckstrand et al., 2010, Varner et al. 2021). The Stordalen mire complex in northern Sweden near Abisko Scientific Research Station offers an excellent opportunity to analyze fluxes from a mire ecosystem with different permafrost and hydrological status: permafrost palsa plateau, thawing bog-like systems, and fully thawed fen systems, at the same climate and weather forcing. Because of the regularity of bi-modal wind directions at Stordalen Mire (Fig. S1,) the footprint areas of the flux measurement can be used to distinguish the fluxes from different ecosystem types.

Most of the published EC studies conducted at Stordalen compare only two stages of permafrost status and focus on methane emission (Jackowicz-Korczyński et al. 2010, Jammet et al. 2017, Lakomiec et al. 2021). Annual averages of CO_2 exchange from a single year presented by Lakomiec et al. (2021) indicated lower net carbon uptake from permafrost areas than from partially thawed area. No comparison between the fen area, and palsa and partially thawed area, based on EC measurements, have been conducted before. In this study we examine how the CO2 exchange at these three systems, and its functional dependencies on light and temperature, differs from each other in order to better understand the C balance of changing Arctic landscapes (Lundin et al. 2016). We can hypothesize that the earlier observed annual methane emissions would scale up with GPP or NEE, that would lead to highest fluxes at the fen site, followed by the partially thawed system and palsa plateau.

2. Materials and Methods

2.1. Study site

The study site, Stordalen Mire (68°21'N, 19°03'E, 360 m als) is a mire complex underlain by discontinuous permafrost situated in Arctic Sweden 10 km east of the village of Abisko (Ábeskovvu). The northern latitudes are exposed to a large temperature increase and the 0 °C threshold for average annual temperature has been exceeded in Abisko since the late 1980s (Callaghan et al., 2013). During the measurement period of this study (2014-2021) mean air temperature was 0.9 °C, while the mean annual temperature for years 1981-2010 was -0.1 °C. Older data (1961-1990) show that the mean annual temperature was -0.9 °C.

The research site is situated within an expansive basin adjacent to Lake Torneträsk (Duortnosjávri). Due to its placement east of the nearby Caledonide mountains precipitation

https://doi.org/10.5194/egusphere-2026-5405
Preprint. Discussion started: 21 September 2026

rates are among the lowest in Sweden due to the rain shadow effect. The average total annual precipitation total during the analyzed period (2014-21), was 295 mm yr^{-1}, while it was 332 mm for years 1981-2010 and around 10% more for the years 1961-1990. The east-west valley of Lake Torneträsk channels the synoptic wind patterns, leading to a bimodal distribution of wind direction (Fig. S1). Unlike at some mountain valleys where the bimodal wind pattern follows a diel cycle, in Abisko-Stordalen the wind pattern is governed by synoptic scale forcing.

The Abisko-Stordalen ICOS Ecosystem station (SE-Sto, www.icos-sweden.se/abisko-stordalen) EC flux tower is located at the border between permafrost palsa plateau and thawing bog-like system. Due to the channeling of the wind, the ICOS SE-Sto flow dataset can be divided into two separate sectors; the western, which is dominated by palsa (underlying permafrost) and the bog-like thawing eastern sector. The lake-shore EC flux system by Jammet et al. (2015, 2017) and Jansen et al. (2019) measured fluxes either from a shallow lake or from a fen system (fully thawed with persistent slow water flow). In this paper only fluxes from palsa sector and partially thawed sector (ICOS tower) and the fen sector (Lake shore tower) are used.

The palsa areas are characterized by the presence of near surface permafrost which lifts the surface to slightly higher elevation (1-2 m), facilitating drainage. Intermediate thawed regions are hydrologically perched above the local water table. *Sphagnum* spp. and other ombrotrophic species are the predominant vegetation. In contrast, fully thawed fen-like areas are lower and are constantly water saturated.

The vegetation on the palsa plateau is dominated by low from ericaceous species such as *Empetrum hermaphroditum*, *Betula nana*, *Rubus chamaemorus*, *Andromeda polifolia, Dicranum* sp. Thawing areas are characterized by ombrotrophic species, such as Eriophorum *vaginatum*, *Carex rotundata*, and cryptogams including *Sphagnum* spp., *Drepanocladus schulzei*, *Polytrichum jensenii* (Johansson et al., 2006). Fen areas have a persistently high-water table level and are dominated by taller macrophytes *Carex rostrate*, Esquisetum spp. and *Eriophorium angustifolium* (Johansson et al., 2006, Jammet et al., 2017; Palace et al., 2018).

2.2. Data

In this analysis we used Swedish national network data from the Integrated Carbon Observation System (ICOS) Ecosystem station Abisko-Stordalen Palsa Bog (station SE-Sto) for the years 2014 to 2021 (ICOS Sweden, 2023; Heiskanen et al., 2022) and data recorded by Jammet et al. (2017) during 2014 (https://fluxnet.org/doi/FLUXNET2015/SE-St1, Running et al., 1999). The data were collected at two separate towers, which were spaced 300 m apart.

2.2.1. Environmental measurements

Abiotic environmental parameters (peat and air temperature, net radiation components, Photosynthetic Photon Flux Density (PPFD), soil heat flux, volumetric soil water content, ground water table, sunshine duration, relative humidity, precipitation) were sampled with the 5 Hz frequency in the air and 1 Hz frequency in the soil and averaged into half-hourly values. Those parameters were measured according to the ICOS instructions (Rebmann et al., 2018). Peat/soil

https://doi.org/10.5194/egusphere-2026-5405
Preprint. Discussion started: 21 September 2026

parameters were measured in the four cardinal directions around the ICOS eddy-covariance tower (SE-Sto) (Fig. 1). In the further analysis only values from palsa and thawing sector location were used. Meteorological parameters in the air were measured at an additional mast north of the ICOS eddy-covariance tower (10 m distance for the years 2014-2017 and 20 m distance since 2018). A detailed list of ancillary parameters is presented by Lakomiec et al. 2021 supplement Table S1. Temperature probes for the fen were installed 5 m south-west of the fen flux tower at 4 different depths (5 cm, 10 cm, 25 cm, and 50 cm). All analyses were based on air temperature and radiation data from SE-Sto data (ICOS Sweden, 2023).

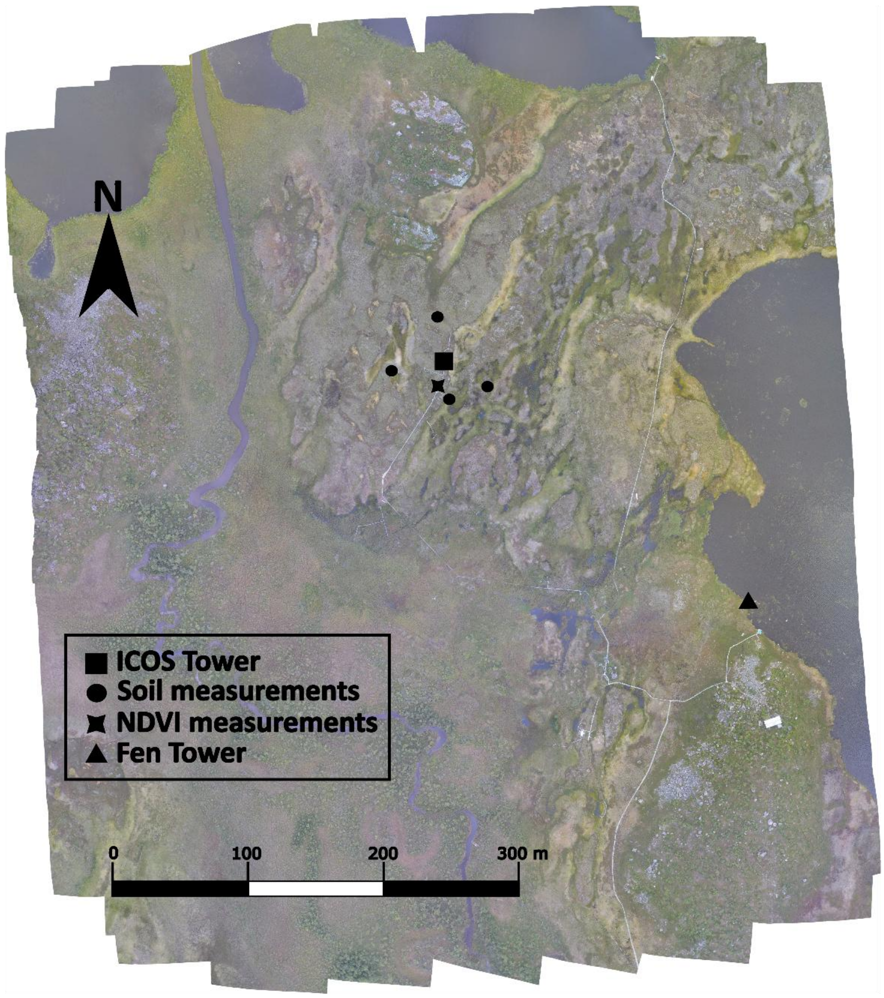

Fig 1. Abisko-Stordalen aerial map with marked ICOS Tower (black square), Soil temperature and measurements (black dots), NDVI measurements (black star), Fen tower (black triangle). Map data retrieved from the SITES Data Portal (https://data.fieldsites.se). SITES, licensed under CC BY 4.0

https://doi.org/10.5194/egusphere-2026-5405
Preprint. Discussion started: 21 September 2026

The normalized difference vegetation index (NDVI eq.1, Rouse et al. 1973) was calculated based on red and near-infrared (NIR) bands of 4-band multispectral sensors (Skye instruments) following methodology in Eklundh et al. (2011). These sensors are mounted on a 20-m tall spectral tower located 35 m south of the ICOS tower (Fig. 1) and included in the SITES Spectral infrastructure. One sensor, fitted with an acrylic cosine diffuser, faces upward to measure incoming light. The second sensor has a 25° field of view and is mounted on a 1-meter boom-oriented westward (300°), looking downward at a 45° off-nadir angle, targeting the palsa area within the ICOS flux footprint

The NDVI is calculated as follows:

$$NDVI = \frac{DVI}{NIR+red} \quad (1),$$

where DVI (difference vegetation index) is given by DVI=NIR−red.

The sensor pair undergoes in-situ calibration every two years, following the method described by Jin and Eklundh (2015).

2.2.2. Eddy-Covariance data

The EC measurements of flux at SE-Sto ICOS tower (Fig. 1) site were made with a LI-COR LI-7200 (LI-COR Environment, USA) enclosed path infrared gas analyzer to measure CO_2 and H_2O and a 3-D sonic anemometer (2014-2017: Metek uSonic-3 CLASS A, Metek GmbH, Germany, 2018 onwards: Gill HS-50, Gill Instruments Ltd.). Air was sampled through 1.05 m by 5.3 mm ID tubing. The sampling inlet was located 22 cm horizontally of the sonic anemometer measurement volume towards the south. The anemometer was pointing towards north. This facilitated uninterrupted airflow from both the palsa plateau and thaw systems. The anemometer together with air sampling tubes were fixed to the mast, at a height of 2.2 m above ground level (a.g.l.). It was situated at the edge of the palsa plateau and thaw system (68°21'21.32" N, 19°2'42.75" E). Data were logged at 20 Hz with an ISDL data logger (In Situ Instrument AB, Sweden) and a CR3000 (Campbell Scientific, Inc., UT, USA).

Data collected at the lake-shore tower 300 m to the southeast at a lake edge by Jammet et al. (2017) were logged on CR3000 (Campbell Scientific, Inc., UT, USA). 3-D sonic anemometer (R3-50, Gill Instruments Ltd.) was mounted on the 2.2 m high mast. Wind components and sonic temperature were sampled at 10 Hz. CO_2 and H_2O were measured with an open path infrared gas analyzer (IRGA) model LI7500 (LICOR Environment, NE, USA) with 10 Hz time resolution. It was mounted at 2.2 m height.

Flux footprint prediction (FFP) model (Kljun et al., 2015) was used to calculate flux footprint for the year 2014 for both towers (Fig. 2). For those calculations data was not divided by the wind sectors.

https://doi.org/10.5194/egusphere-2026-5405
Preprint. Discussion started: 21 September 2026

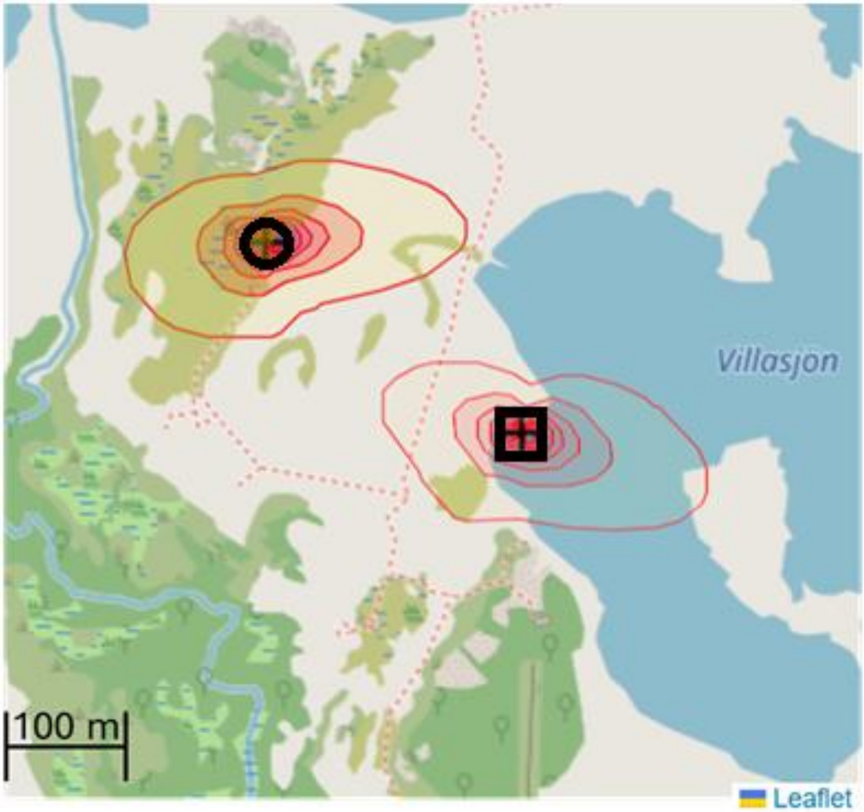

Fig 2. Abisko-Stordalen map with the flux footprint calculation, where circle shows ICOS Tower and square shows Fen Tower.

As in Lakomiec et al. (2021), the datasets were divided into the two wind sectors and analyzes were done separately for each sector: For SE-Sto, the wind direction sector 225°-315° was dominated by the drained, drier permafrost palsa plateau located to the west of the EC mast, hereafter called as the palsa plateau. Wind directions from 45°-135° represented the thawing bog-like collapsing palsa area underlain by discontinuous permafrost, referred hereafter as the thawing system, to the east of the SE-Sto mast with mixture of the thawing segments and palsas, each comprising about 50% to the area. The lake-shore tower was located at a lake edge between open water and a fen to the west. Jammet et al., (2015) used a slightly wider range for the wind rose sectors 20°–135° and 210°–330°. We used a narrower wind sector of 45° to 135° to isolate the fluxes originating from the fen area laying to the west of the tower. Data for 2020 from SE-Sto were not used because of technical problems with the installations.

Low turbulence conditions were not observed in the data, because it related to Northerly and Southerly winds and those data were outside the selected wind sectors. The CO_2 fluxes were not sensitive to conditions with low turbulence, identified with low friction velocity u* (below 0.6 m s^{-1}). Thus, no u* filtering of nighttime fluxes was needed.

https://doi.org/10.5194/egusphere-2026-5405
Preprint. Discussion started: 21 September 2026

Datasets were divided into daytime (PPFD ≥ 50 µmol m^{-2} s^{-1}) and nighttime (PPFD < 50 µmol m^{-2} s^{-1}). Additionally, for PPFD higher than 800 µmol m^{-2} s^{-1}, CO_2 fluxes were considered as light saturated, with no further increase of the CO_2 uptake with higher PPFD.

Temperature and light conditions control much of the variation of CO_2 exchange between ecosystems and atmosphere (Pugh et al., 2018, Runkle et al., 2012). We analyzed the light and temperature responses of CO_2 exchange from the three selected sectors by fitting well known response functions: for the light response, the rectangular hyperbolic model (Eq. 2, Michaelis-Menten, Falge et al., 2001) was used; for the temperature response fitting coefficients to an exponential function (Eq. 3, Van't Hoff, Kutzbach et al., 2007) were calculated. Calculations were done with a two-week window length, which was moved one week to maximize the number of available data points, like moving averaging function.

$$NEE= Rday - \frac{b_1 * b_2 * PPFD}{b_1 * PPFD + b_2} \qquad (2)$$

Here b_1 is the slope which shows light use efficiency (LUE) for photosynthesis, b_2 is the saturation level for the CO_2 flux, b_3 is the daytime respiration, and PPFD is the incoming PPFD.

$$Reco = c_1 * e^{c_2 T} \qquad (3)$$

with nighttime respiration Reco, empirical scaling factors c_1 and c_2, and air temperature T.

2.3. Data gap-filling

The three-time series were gap-filled for calculation of annual sums of CO_2 exchange. Most of the recent EC studies use more than one gap-filling method (Kim et al. 2019, Irvin et al. 2021). As in Lakomiec et al. (2021) three different methods were used here: REddyProc (Wutzler et al. 2018), artificial neural network (ANN, e.g. Walczak & Cerpa 2003), and generalized linear models (GLM, e.g. Rinne et al. 2018). Gap-filling used half-hourly means due to the pronounced diurnal cycle in the CO_2 flux. The use of several gap-filling methods minimizes uncertainty in the annual balance calculation that would occur if only one method was used. This is especially crucial for this study, as the division of the data to two sectors lowers the number of available datapoints per sector.

REddyProc uses half-hourly binned CO_2 fluxes and environmental parameters (shortwave incoming radiation, air temperature, soil temperature, relative humidity, and friction velocity). Data gaps are filled by half-hourly mean flux value, calculated from available fluxes under similar environmental conditions using look-up tables, mean daily cycles and marginal distribution sampling. The same fluxes are used for the calculation of standard deviation. The method is fully presented and described by Falge et al. (2001), Reichstein (2005), and Wutzler et al. (2018).

The ANN was calculated in MATLAB using the fitnet function (https://uk.mathworks.com/help/deeplearning/ref/fitnet.html) with 30 hidden neurons. The Levenberg-Marquardt algorithm was used as a training function (Levenberg 1944, Marquardt 1963). The full dataset of available half-hourly CO_2 fluxes was randomly split for training (70%), validating (15%), and testing (15%). Input for the ANN is presented in Table S1. Data gaps in the

https://doi.org/10.5194/egusphere-2026-5405
Preprint. Discussion started: 21 September 2026

environmental data were filled by linear interpolation between points. 100 repetitions for each sector and year were performed to obtain consistent statistical characterization of the output. The filled half-hour value was calculated as the average over all repetitions. Uncertainties were calculated as a standard deviation over all repetitions.

The generalized linear models (GLM) method examines the dependence of response variables (half-hour CO_2 flux) on predictors (listed in Table S1). Dependences are described as linear combinations of linear and quadratic functions. Data gaps in the predictors' time series were filled by linear interpolation. The *stepwiseglm* function from MATLAB (Dobson 2002), gives predicted value and confidence intervals.

Gap-filled CO_2 fluxes were partitioned into the GPP and Reco using the day-time flux partitioning method in the ReddyProcWeb online tool (Wutzler et al., 2018, Lasslop et al. 2010). In this method GPP and Reco are model predictions thus their sum is not always exactly equal to the measured CO_2 fluxes.

3. Results and discussion

3.1. Environmental conditions

Incoming PPFD peaked around mid-June with half hourly levels around 1800 umol m^{-2} s^{-1} (Fig. 3). During the summer, PPFD levels are sufficiently high to support efficient photosynthesis and enhance CO_2 uptake. The light regime is determined by the geographical location of Stordalen Mire, which lies north of the polar circle resulting in the sun above the horizon 24 hours per day from 23 May until 19 July. In contrast, the situation takes a different turn during the winter period, when the sun is below the horizon 24 hours pers day from 8 Dec until 4 Jan. The growing season, frozen soil season, and unfrozen soil season were defined as in Lakomiec et al. (2021). Outgoing, i.e. reflected PPFD was typically high at the beginning of the unfrozen season when the ground was still covered by snow/ice and incoming solar radiation, and sun angles were already high. Maximum reflected PPFD occurred in mid-April. The lowest maximum of the outgoing PPFD was observed in the year 2016 and was earlier, mid-March, decreasing later indicating shorter snow-covered period during this year. Snow/ice cover built up earlier in 2019, as indicated by an increase of the outgoing radiation at the end of the year (Fig. 3), compared to other years.

https://doi.org/10.5194/egusphere-2026-5405
Preprint. Discussion started: 21 September 2026

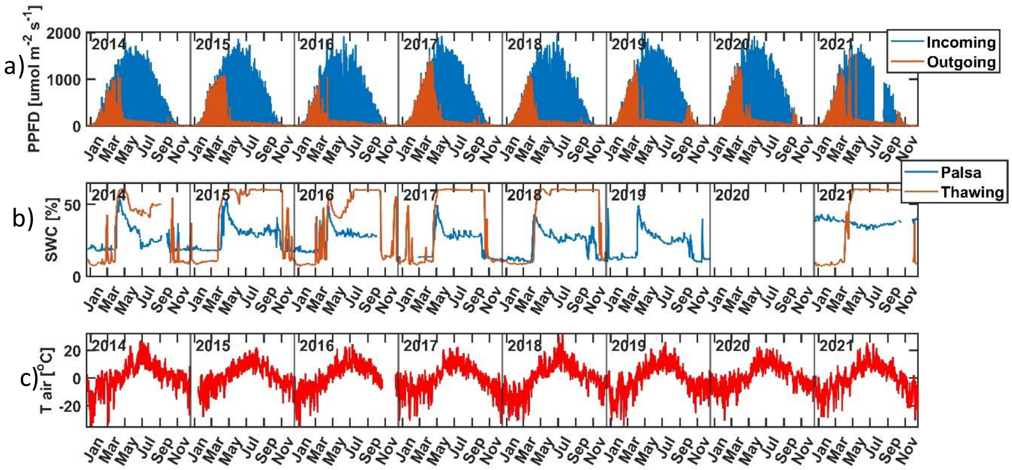

Fig 3. Time series of ecosystem variables. Top panel presents incoming PPFD (blue) and outgoing PPFD (orange). Middle panel presents SWC for the palsa sector (blue) and thawing sector (orange). Bottom panel shows air temperature. Grey lines represent start of the new year.

Earlier snow melt in 2016 compared to the other years had significant impact on the vegetation development. The annual cycle of NDVI is characterized by very low values in winter due to snow, then a steep increase as snow melts followed by a gradual increase in spring during the green-up phase of vegetation (Eklundh et al. 2011). This springtime increases in NDVI started around one month earlier in 2016 (DOY 150) than in the other years and NDVI reached the maximum value of approximately 0.72 around DOY 180 (Fig. 4). Around DOY 180, NDVI for other years was around 0.68.

https://doi.org/10.5194/egusphere-2026-5405
Preprint. Discussion started: 21 September 2026

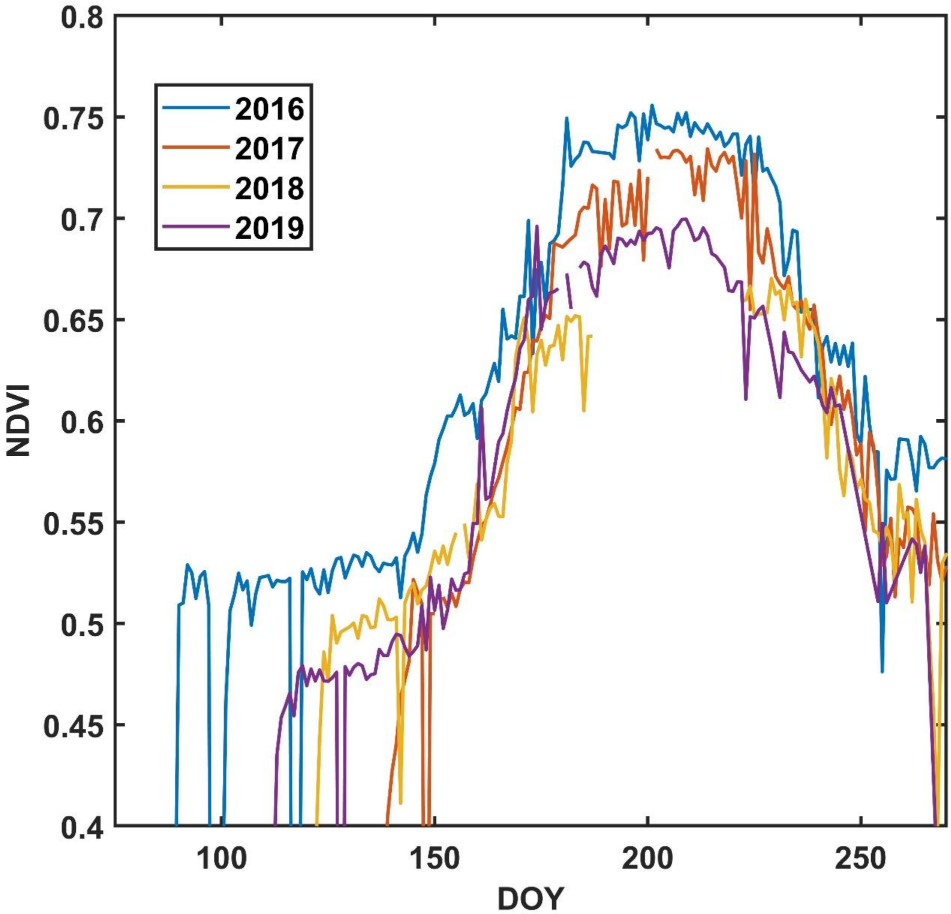

Figure 4. NDVI for the years 2016-2019.

Early snowmelt in 2016 is also discernible in the albedo data. In the year 2016, snowmelt is observable approximately one month in advance compared to other years. During this particular year, a reduction in albedo is noted around DOY 90, whereas the decline in albedo in other years typically occurs around DOY 120 (Fig. S2).

Soil water content (SWC) in peat differed between the palsa and the thawing sectors (Fig. 3). For most of the unfrozen period the thawing sector peat was fully saturated to 6 cm in depth. Peat in the palsa plateau was drier and not fully saturated during any period though still moist. SWC for the fen was not measured but the water table was always very close to or above the peat surface. Unlike in many other mire ecosystems in Fennoscandia (Rinne et al. 2020), drought conditions were not observed at Abisko-Stordalen during summer 2018. In 2020 SWC data is missing due to sensor failure.

https://doi.org/10.5194/egusphere-2026-5405
Preprint. Discussion started: 21 September 2026

During 2014, the only year with flux data from the fen, the annual peat temperature in all depths in fen (5 cm, 10 cm, 25 cm, and 50 cm) was higher than in the two other systems. The largest difference in the peat temperature between fen and two other sectors was observed at the 50 cm depth, due to thawed permafrost. The average peat temperature during frozen period in palsa was colder for all analyzed years.

The average air temperature during the frozen period was lowest during the year 2018 (-13.7 °C), while multiyear (2014-2021) average was -8.9 °C. During the unfrozen period, average air temperature (Fig. 3) was the highest for the year 2014 (13.5 °C) and then for 2018 (12.7 °C) while other analysed years (2015-2021 without 2018) average was 11.2 °C. The second highest unfrozen period air temperature was connected to the heatwave in summer 2018, to which most of north-western Europe was exposed (El-Madany et al., 2020, Peters et al., 2020, Rinne et al., 2020). SWC in 2018 did not show any differences compared to other years. Despite the increase in the air temperature, drought conditions were not observed.

3.2. NEE

At the ICOS tower, air flowed 87±2% of the time from the two specified (East and West) wind sectors which follows the same pattern observed in 2014-16 by Lakomiec et al. (2021). Wind from outside the two dominant wind direction sectors were usually related to the conditions with low wind speeds (below 3 ms $^{-1}$).

CO_2 fluxes showed similar interannual variability in palsa and the thawing systems (Fig. 5). The maximum CO_2 uptake was observed in late July, where weekly multiyear average NEE were -3.5 µmol m^{-2} s^{-1} and -3.3 µmol m^{-2} s^{-1} at the thawing sector and palsa plateau, respectively (Fig. S3). The maximum in the weekly multiyear average nighttime NEE was observed slightly later, around early August, with 2.1 µmol m^{-2} s^{-1} for the thawing system and 2.4 µmol m^{-2} s^{-1} at the palsa plateau. The lag between maximum uptake and maximum release could relate to higher peat temperature at deeper parts (Wu et al. 2021).

https://doi.org/10.5194/egusphere-2026-5405
Preprint. Discussion started: 21 September 2026

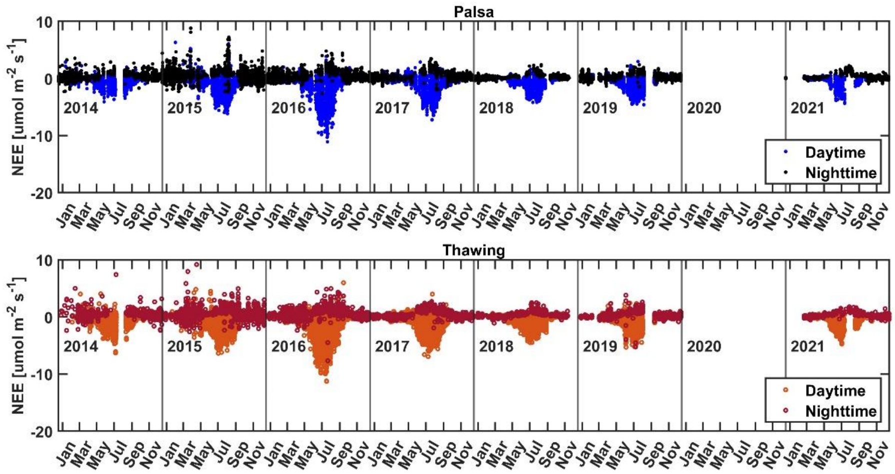

Figure 5. Time series of the half-hour CO_2 fluxes divided during daytime (PPFD>=50) fluxes and nighttime (PPFD<50) fluxes. Upper panel shows palsa sector daytime (blue) and nighttime (black) for the years 2014-2021, bottom panel shows thawing sector daytime (orange) and nighttime (red) for the years 2014-2021. Grey lines represent start of the new year.

For 2014, CO_2 flux data from all three systems, palsa plateau, thawing area and fen, were available (Fig. 6). The maximum CO_2 uptake was observed at all systems in late July. At the fen site the maximum weekly average NEE was -7.6 umol m^{-2} s^{-1}, compared to -1.6 umol m^{-2} s^{-1} at the palsa and -2 umol m^{-2} s^{-1} into the thawing area. The highest weekly average nighttime respiration at the fen was 3.2 umol m^{-2} s^{-1}, compared to 1.9 umol m^{-2} s^{-1} at palsa plateau and 1.2 umol m^{-2} s^{-1} at thawing sector. The maximum respiration was observed around early August as in the other systems. The significance of the differences between those systems were tested separately for the nighttime and daytime light-saturated fluxes. Weekly average light-saturated CO_2 fluxes at fen system were significantly different from those at the palsa and thaw systems for most of the time during 2014. Between the palsa and thawing system the differences between CO_2 fluxes were mostly not significant. However, in each year, some weeks show significant differences ($p<0.001$, two-sided Wilcoxon rank sum test) but the periods when systematic differences occurred varied from year to year. Those differences occurred randomly in each year. Weekly averages of night-time CO_2 fluxes were significantly different for the growing season between fen and palsa and between fen and thawing sector (Fig. S4).

https://doi.org/10.5194/egusphere-2026-5405
Preprint. Discussion started: 21 September 2026

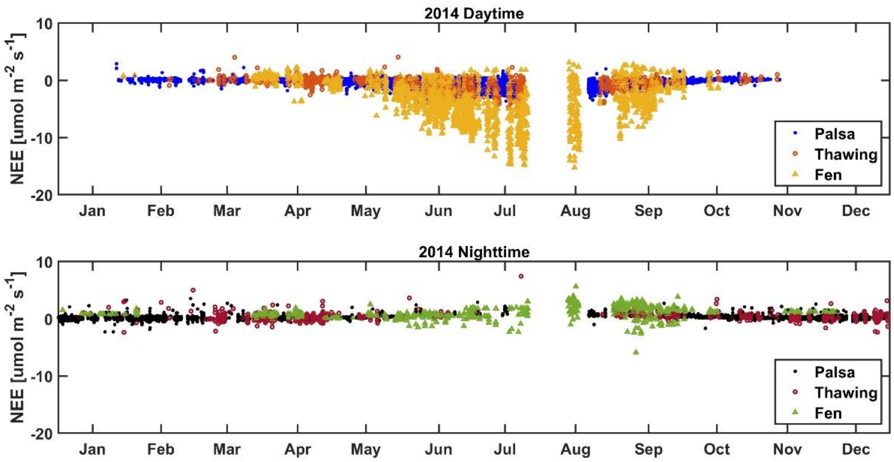

Figure 6. Time series of the half-hour CO_2 fluxes divided during daytime (PPFD>=50) fluxes and nighttime (PPFD<50) fluxes observed at the two towers in 2014. Upper panel shows palsa sector (blue), thawing sector (orange) and fen (yellow) for the daytime the year 2014. Bottom panel shows palsa (black), thawing (red) and fen (green) sector for the daytime for the year 2014.

Frozen period palsa and thawing sector half-hour NEE were significantly different from zero ($p<0.001$, two-sided Wilcoxon rank sum test) during most of the years. No significant difference from zero was observed during years 2014 and 2019. However, the number of available wintertime data points for these years was much lower than for the other years which could have impacted the result of the statistical test.

The highest weekly average uptake and release of CO_2 from palsa and partially thawed sector was observed during year 2016. It is worth noting that the meteorological conditions during this particular year differed significantly from those observed in other years. Specifically, the daily average air temperature after day 116 was notably higher in 2016 compared to the multiyear average (Fig. S5). Moreover, the peak of the PPFD occurred approximately one month earlier in 2016 compared to other years. Between DOY 85 and DOY 95, net longwave radiation was higher in 2016 compared to the other years. This suggests reduced cloud cover during this period, potentially contributing to the unusually warm and snow-deficient spring conditions. Similarly, the decrease in the outgoing PPFD, indicating snow free conditions, at the beginning of the year started about a month earlier compared to previous years. NDVI this year was also higher than in other years (Fig. 4). These factors played a pivotal role in prolonging the unfrozen period and consequently resulted in higher GPP. In ecosystems such as Abisko, where the growing season is short (ca. 40 days), any alteration in the length of the unfrozen period can have a substantial impact on vegetation and fluxes (Aurela et al. (2004), Rafat et al. (2022)). The remaining years were comparatively similar in terms of these parameters.

https://doi.org/10.5194/egusphere-2026-5405
Preprint. Discussion started: 21 September 2026

The half-hourly non-gap-filled NEE at all the three mire surfaces had qualitatively similar diel cycles with net CO_2 uptake in daytime and net respiration during nighttime (Fig. 7 and S6). In June and July, Reco remained consistent across all three systems. In August, Reco was substantially higher in the fen. Daytime CO_2 uptake in the fen was nearly three times greater than that observed in the palsa and thawing systems. The daily uptake period was around 18h per day for June, 20h per day for July and 14h per day for August. The length of the daily uptake period and shortness of the net respiration period reflects the radiative conditions at this high latitude site (e.g. Taillardat et al. 2022). Especially in June the period of daylight during the summer is long and night is short, but soil temperatures are cooler than July and August. During the year 2014, when data exists from all three systems, the daytime net CO_2 uptake in fen is 3-4 times higher than that from palsa plateau and thawing systems. During this year the frozen and snow period was the longest in the palsa plateau sector. Low nighttime respiration rates were observed at all three systems in the beginning of growing season (June), while later in the season (August), the nighttime respiration at the fen is much higher than at palsa plateau or thaw system. NEE at palsa and the thawing systems had very similar diel cycle throughout most of measurement years.

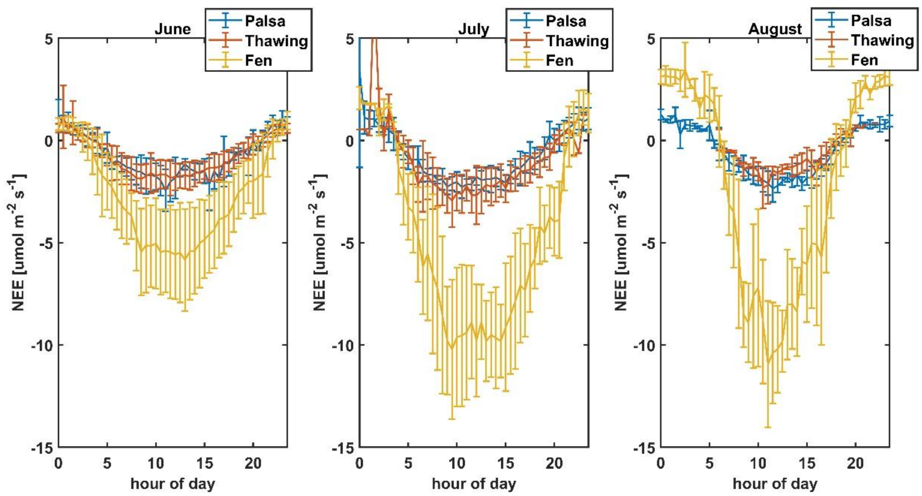

Figure 7. Diel cycle of the CO2 fluxes for the june (left panel), july (middle panel) and august (right panel) for the palsa (blue), thawing sector (orange) and fen (yellow) for the year 2014

The analysis of light response curves shows no differences between palsa and thawing sectors. The fen showed higher response to light, with CO_2 uptake varying depending on the PPFD range, reaching values up to eight times greater than those observed in the other two sectors (Fig. 8). The light response curves at palsa and partially thawed sectors for the year 2016 do not correspond with the light response curves for other years based on the fit parameters uncertainty (Fig. 9). Within that particular year, the light response curves for these sectors exhibit agreement with each other. For the multiyear dataset, the NEE during light-saturated conditions did not

https://doi.org/10.5194/egusphere-2026-5405
Preprint. Discussion started: 21 September 2026

differ significantly between palsa and partially thawed systems, with mean values of 4.1 µmol CO_2 m^{-2} s^{-1} in the thawing sector and 4.0 µmol CO_2 m^{-2} s^{-1} on the palsa. However, in the specific year 2016, both areas exhibited significantly higher saturation-level NEE, measuring 9.0 µmol CO_2 m^{-2} s^{-1} in the thawing sector and 8.9 µmol CO_2 m^{-2} s^{-1} on the palsa.

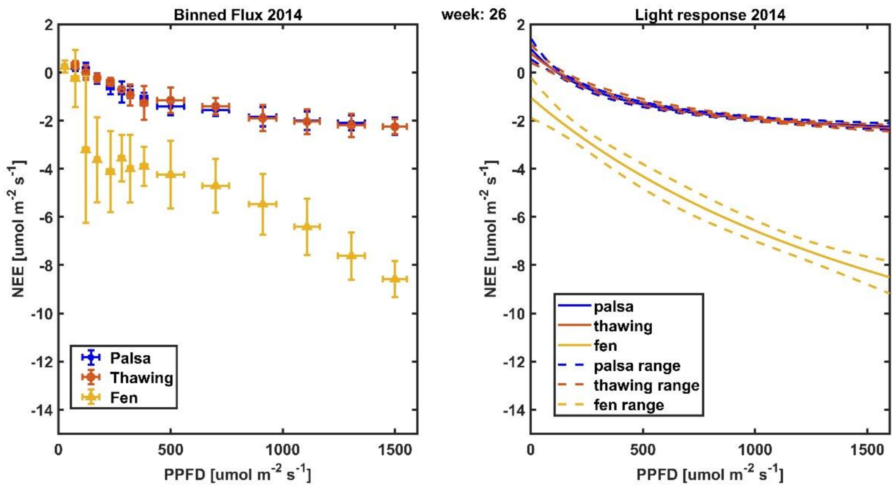

Figure 8. Left panel presents binned CO2 daytime fluxes for year 2014 for the palsa sector (blue), thawing sector (orange) and lake edge tower fen sector (yellow). Right panel presents light response curves (solid lines) with the uncertainties (dashed lines) for the year 2014. Both panels show data from the week 26.

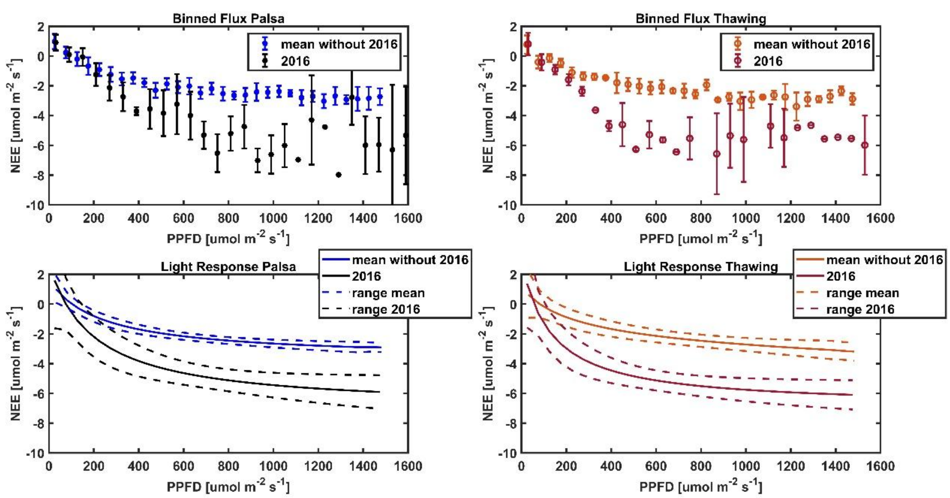

Figure 9. Binned CO2 daytime fluxes for week 28 with the mean and standard deviation for the palsa (left top panel) and thawing sector (right top panel) and light response curves (solid lines) with the uncertainties (dashed lines) of the fit for the palsa sector (left bottom panel) and thawing sector (right bottom panel).

https://doi.org/10.5194/egusphere-2026-5405
Preprint. Discussion started: 21 September 2026

Increased photosynthesizing biomass, resulting from an earlier onset of the snow-free period, may have led to a stronger ecosystem response to light in 2016 compared to other years. The observation of the light response suggests that temporal variations in daytime NEE (Fig. 5) are not directly attributable to differences in PPFD or temperature, but rather to the increased presence of photosynthetic biomass.

We also analyzed the response of nighttime fluxes to the air temperature. The location of Abisko north of the polar circle limits the number of nighttime hours during the growing season. Fitted curves are highly uncertain due to fewer available data points and high scatter. Despite that, we observe agreement for the palsa and thawing sectors and significant difference for the fen from those two sectors for the year 2014 (Fig. 10). For the multi-year analysis, response for the year 2016 is slightly higher than for other years for palsa and partially thawed sectors (Fig. 11). The nighttime response agrees for palsa and thawing sector for the year 2016. Reco is higher for the year 2016 compared to other years and it relates to increased plant development (Fig. 4). Confidence intervals for all years are large due to few data for fitting the algorithm. Additionally, the range of fluxes for the fitting is relatively low which also has impact on the high uncertainties.

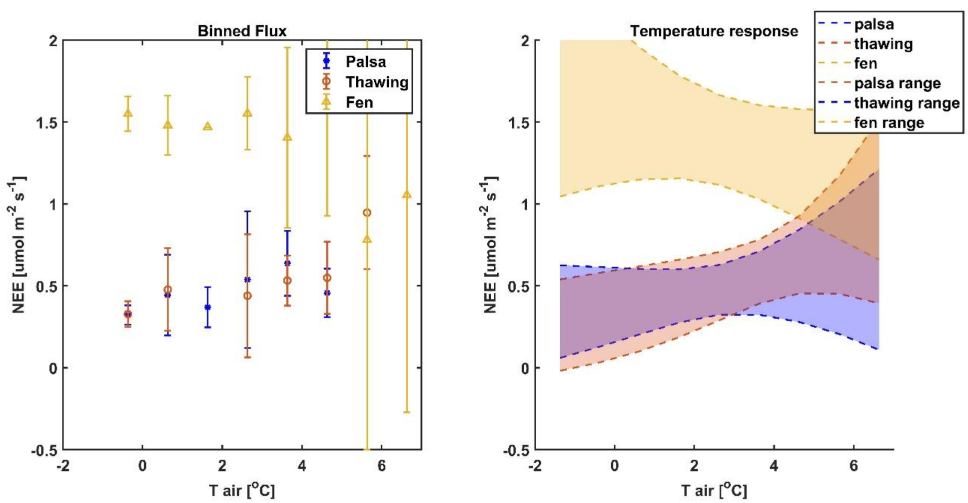

Figure 10. Left panel presents binned CO2 nighttime fluxes for year 2014 for the palsa sector (blue), thawing sector (orange) and lake edge tower fen sector (yellow). Right panel presents air temperature response curves with the uncertainties (dashed lines). Both panels show data from week 39.

https://doi.org/10.5194/egusphere-2026-5405
Preprint. Discussion started: 21 September 2026

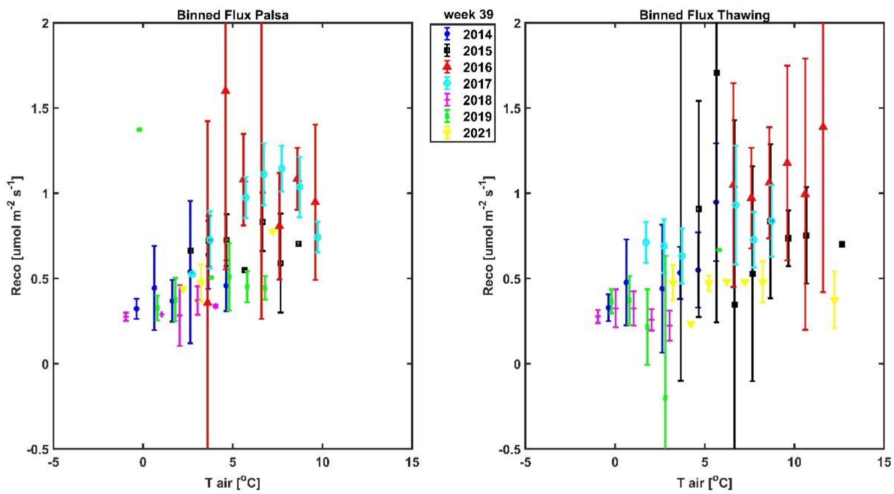

Figure 11. Binned CO_2 nighttime fluxes for the week 39 with the mean and standard deviation for the palsa (left panel) and thawing sectors (right panel). Each color indicates one year presented in the legend.

3.3. Annual carbon balances

Annual CO_2 balance for the palsa and the thawing sectors for each method for years 2014-2021 is presented in Table S2. The highest yearly uptake of CO_2 is estimated for the year 2016, which was described as the year with the longer growing season. The lowest yearly uptake or even release of CO_2 is estimated for the year 2014. Gap-filling methods do not lead to differences in the estimation of the annual budget.

The annual NEE for the fen was calculated only for the year 2014 (Table S2). NEE for this sector is much higher than for the other two sectors for all the three methods. Moreover, mean estimated value is higher than one presented by Jammet et al. 2017. In the Jammet et al. 2017 study, uncertainty of approximately 100 gC m-2 y-1 was reported.

An estimated annual NEE for the palsa and thawing bog were subtracted from each other for each year and method. This was done to compare which ecosystems have higher NEE and analyze how different methods are estimated differences. All methods agree that the palsa had stronger CO_2 uptake than the thawing sector during year 2014, compared to the other years. Stronger uptake for the thawing sector than for the palsa is observed for the 2019 and 2021. The estimation based on three methods for other years is not in agreement regarding which sector has stronger uptake.

The ANN data series were chosen for partitioning NEE into GPP and Reco. The ANN method was successfully tested and used in many different study cases (e.g. Lucas-Moffat et al. 2022, Jasek-Kamińska et al. 2024). These data series were chosen to avoid bias connected with using the

https://doi.org/10.5194/egusphere-2026-5405
Preprint. Discussion started: 21 September 2026

same variables and equations that is used for the partitioning. Additionally, averaging over 100 repetitions also should minimize the bias caused by different usage of parameters and randomization of parameters. Annual cumulative sums of GPP and Reco are presented on Fig. 12. The most visible differences in the GPP between the palsa plateau and thawing sector were observed in years 2016 and 2021, with palsa plateau has higher GPP. Furthermore, mean Reco was slightly higher at palsa plateau in years 2015, 2019 and 2021 but the differences were not significant. Fen GPP and Reco for year 2014 (Fig. S7) are significantly higher than GPP and Reco for palsa and thawing sector.

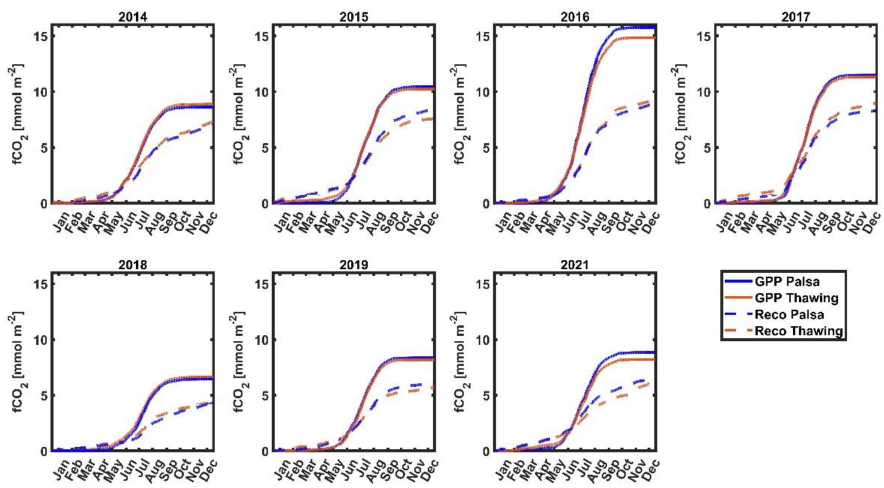

Figure 12. Cumulative sum of the ANN gapfilled CO_2 fluxes partitioned for the GPP and Reco for the years 2014-2021 (without 2020). Solid lines present GPP for palsa secor (blue) and thawing sector (orange) and dashed lines present Reco for palsa (blue) and thawing (orange) sectors.

Multiyear average GPP is 195 ± 36 gC m^{-2} y^{-1} for palsa and 192 ± 30 gC m^{-2} y^{-1} for the thawing sector. While Reco is 146 ± 33 gC m^{-2} y^{-1} and 146 ± 35 gC m^{-2} y^{-1}, respectively for palsa and thawing sector. Sector differences observed in the average annual NEE by Lakomiec et al. (2021) were likely an effect of the gap-filling method and averaging with the year 2016. Lakomiec et al. (2021) assumed that three-year period is comparable to each other in terms of fluxes, especially that CH_4 fluxes do not show big difference to each other in comparison with those of CO_2 fluxes. Like the reported methane emissions, the fen showed largest annual NEE, GPP and Reco. However, the annual NEE or the GPP do not show similar differences between palsa plateau and thaw bog as do their methane emissions reported by Lakomiec et al. (2021).

Yearly NEE with the standard deviation based on the three gap-filling models are presented in the Fig 13. The fen sector had a significantly higher annual CO_2 uptake than other areas in the year 2014, for which data from all three surfaces was available. Emissions for the year 2014 for the thaw sector suggest release of CO_2 instead of uptake, and this is the only year that ecosystem

https://doi.org/10.5194/egusphere-2026-5405
Preprint. Discussion started: 21 September 2026

behaves as a weak source instead of a sink. The multiyear average annual balance was calculated without data from year 2016, which is significantly higher. The average annual balance is -31 ± 7 gC m^{-2} y^{-1} for the palsa and -31 ± 6 gC m^{-2} y^{-1} for the thawing sector.

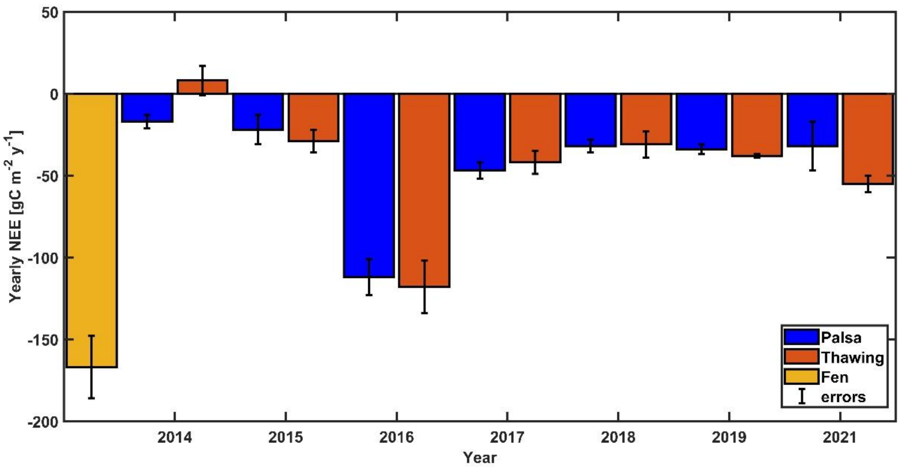

Figure 13. Average annual NEE with the standard deviation calculated based on the three models (ANN, GLM, Jena).

Observed NEE at the Fen site in this study demonstrates a significantly higher carbon uptake compared to other sites presented in Table 1, excluding the palsa and thawing sectors for the year 2016. Among presented sites, the Kobbefjord Fen has the lowest net carbon uptake and very different plant community. This is followed by the palsa and thawing permafrost sectors when considering the multiyear dataset.

Table 1. Mean yearly NEE (average from all methods) for this study and values reported in the literature

Site	NEE [gC m^{-2}]	Cite
Fen	-167	This study
Thawing sector multiyears	-31	This study
Palsa multiyears	-31	This study
Thawing sector 2016	-117	This study
Palsa 2016	-112	This study
Zackenberg	-50	López-Blanco et al. 2020
Degerö	-56	Yurova et al. 2007
Kobbefjord Fen	-18	López-Blanco et al. 2020
Siikaneva fen	-50	Rinne et al. 2018
Schechenfilz	-62	Hommeltenberg et al. 2014

In contrast, the remaining sites listed in Table 1 consistently display substantially greater carbon uptake relative to the palsa and thawing permafrost areas. However, NEE estimated for the palsa and thawing sectors in the year 2016 are significantly higher than those measured at other fen sites. This suggests that

https://doi.org/10.5194/egusphere-2026-5405
Preprint. Discussion started: 21 September 2026

the carbon uptake observed in 2016 for these sectors represents an anomaly, underscoring extraordinary situation, indicating environmental conditions during that year.

Overall, our results indicate that to understand the surface-atmosphere exchange of carbon in the rapidly changing margins of the Arctic, we need to obtain data that covers both the interannual variability of the fluxes and small-scale spatial variability. Additional data, such as NDVI, can provide essential tools to understand the interannual variability of these fluxes.

4. Conclusions

As expected, the fen system exhibited the highest CO_2 uptake and GPP of the three systems studied. However, contrary to our expectations the palsa plateau and the partially thawed bog exhibited no significant differences in their NEE or GPP, despite them has different permafrost conditions, soil moisture levels, vegetation characteristics, and annual methane emission, (Lakomiec et al 2021). Furthermore, it was shown that response GPP and Reco to light and temperature at the palsa plateau and the thaw bog were not significantly different, whereas at the fen system the response of GPP to the light was stronger, with much higher light saturated GPP.

Of the three types of surfaces that were examined in this study the fen exhibited the largest uptake of CO_2 during daytime in the summer season. Furthermore, as the growing season progressed, it also displayed the largest net respiration during nighttime.

The fluxes of CO_2 in the anomalous year 2016 at palsa plateau and partially thawed bog deviated considerably from those of the other years. This could be attributed to the earlier melting of the snow and ice cover, resulting in an extended period of vegetation growth, potentially leading to an increase in phytomass, as indicated by the higher NDVI in this year, and subsequently a higher uptake of CO_2. Conversely, the remaining years exhibited a similar range of fluxes.

Author contribution

PŁ, JH, TF, PC, ER, and JR analyzed and interpreted the data. PŁ, JH, PC, ER, and JR wrote the manuscript. TF, PC, ER, and NR designed the measurements. HJ and LE were responsible for interpreting NDVI data.

Competing interests

The authors declare that they have no conflict of interest.

Acknowledgements

This study has been made possible by the Abisko Scientific Research Station (ANS), theSwedish Infrastructure for Ecosystem Sciences (SITES)and ICOS Sweden. Both ICOS and SITES have been co-financed by the Swedish Research Council.

This research leading to these results has received funding from the European Union's Horizon 2020 research and innovation program under the Marie Skłodowska-Curie grant no. 722479 (MEthane goes Mobile: MEasurement and MOdeling - MEMO2) and "Greenhouse Gas Fluxes and Earth System

Feedbacks" (GreenFeedBack) project from the European Union's Horizon Europe Framework Programme for Research and Innovation (project no. 101056921).

Disclaimer: The views and opinions expressed are those of the author(s) only and do not necessarily reflect those of the European Union. Neither the European Union nor the granting authority can be held responsible for them.

References

Åkerman, H. J. and Johansson, M.: Thawing permafrost and thicker active layers in sub-arctic Sweden, Permafr Periglac Process, 19, 279–292, https://doi.org/10.1002/ppp.626, 2008.

Aurela, M., Laurila, T., and Tuovinen, J.: The timing of snow melt controls the annual CO2 balance in a subarctic fen, Geophys Res Lett, 31, https://doi.org/10.1029/2004GL020315, 2004.

Bäckstrand, K., Crill, P. M., Mastepanov, M., Christensen, T. R., and Bastviken, D.: Total hydrocarbon flux dynamics at a subarctic mire in northern Sweden, J Geophys Res Biogeosci, 113, https://doi.org/10.1029/2008JG000703, 2008.

Bäckstrand, K., Crill, P. M., Jackowicz-Korczyñski, M., Mastepanov, M., Christensen, T. R., and Bastviken, D.: Annual carbon gas budget for a subarctic peatland, Northern Sweden, Biogeosciences, 7, 95–108, https://doi.org/10.5194/bg-7-95-2010, 2010.

Biskaborn, B. K., Smith, S. L., Noetzli, J., Matthes, H., Vieira, G., Streletskiy, D. A., Schoeneich, P., Romanovsky, V. E., Lewkowicz, A. G., Abramov, A., Allard, M., Boike, J., Cable, W. L., Christiansen, H. H., Delaloye, R., Diekmann, B., Drozdov, D., Etzelmüller, B., Grosse, G., Guglielmin, M., Ingeman-Nielsen, T., Isaksen, K., Ishikawa, M., Johansson, M., Johannsson, H., Joo, A., Kaverin, D., Kholodov, A., Konstantinov, P., Kröger, T., Lambiel, C., Lanckman, J. P., Luo, D., Malkova, G., Meiklejohn, I., Moskalenko, N., Oliva, M., Phillips, M., Ramos, M., Sannel, A. B. K., Sergeev, D., Seybold, C., Skryabin, P., Vasiliev, A., Wu, Q., Yoshikawa, K., Zheleznyak, M., and Lantuit, H.: Permafrost is warming at a global scale, Nat Commun, 10, https://doi.org/10.1038/s41467-018-08240-4, 2019.

Burke, E. J., Ekici, A., Huang, Y., Chadburn, S. E., Huntingford, C., Ciais, P., Friedlingstein, P., Peng, S., and Krinner, G.: Quantifying uncertainties of permafrost carbon-climate feedbacks, Biogeosciences, 14, 3051–3066, https://doi.org/10.5194/bg-14-3051-2017, 2017.

Callaghan, T. v., Bergholm, F., Christensen, T. R., Jonasson, C., Kokfelt, U., and Johansson, M.: A new climate era in the sub-Arctic: Accelerating climate changes and multiple impacts, Geophys Res Lett, 37, https://doi.org/10.1029/2009GL042064, 2010.

Callaghan, T. v, Jonasson, C., Thierfelder, T., Yang, Z., Hedenås, H., Johansson, M., Molau, U., van Bogaert, R., Michelsen, A., Olofsson, J., Gwynn-Jones, D., Bokhorst, S., Phoenix, G., Bjerke, J. W., Tømmervik, H., Christensen, T. R., Hanna, E., Koller, E. K., and Sloan, V. L.: Ecosystem change and stability over multiple decades in the Swedish subarctic: complex processes and multiple drivers,

https://doi.org/10.5194/egusphere-2026-5405
Preprint. Discussion started: 21 September 2026

Philosophical Transactions of the Royal Society B: Biological Sciences, 368, 20120488, https://doi.org/10.1098/rstb.2012.0488, 2013.

Chen, Y., Lara, M. J., Jones, B. M., Frost, G. v., and Hu, F. S.: Thermokarst acceleration in Arctic tundra driven by climate change and fire disturbance, One Earth, 4, 1718–1729, https://doi.org/10.1016/j.oneear.2021.11.011, 2021.

Christensen, T. R., Johansson, T., Åkerman, H. J., Mastepanov, M., Malmer, N., Friborg, T., Crill, P., and Svensson, B. H.: Thawing sub-arctic permafrost: Effects on vegetation and methane emissions, Geophys Res Lett, 31, https://doi.org/10.1029/2003GL018680, 2004.

Crowther, T. W. and Bradford, M. A.: Thermal acclimation in widespread heterotrophic soil microbes, Ecol Lett, 16, 469–477, https://doi.org/10.1111/ele.12069, 2013.

Dobson, A. J.: An introduction to generalized linear models/Annette J. Dobson, Chapman & Hall/CRC, Boca Raton, 2002.

El-Madany, T. S., Carrara, A., Martín, M. P., Moreno, G., Kolle, O., Pacheco-Labrador, J., Weber, U., Wutzler, T., Reichstein, M., and Migliavacca, M.: Drought and heatwave impacts on semi-arid ecosystems' carbon fluxes along a precipitation gradient, Philosophical Transactions of the Royal Society B: Biological Sciences, 375, 20190519, https://doi.org/10.1098/rstb.2019.0519, 2020.

Falge, E., Baldocchi, D., Olson, R., Anthoni, P., Aubinet, M., Bernhofer, C., Burba, G., Ceulemans, R., Clement, R., Dolman, H., Granier, A., Gross, P., Grünwald, T., Hollinger, D., Jensen, N.-O., Katul, G., Keronen, P., Kowalski, A., Lai, C. T., Law, B. E., Meyers, T., Moncrieff, J., Moors, E., Munger, J. W., Pilegaard, K., Rannik, Ü., Rebmann, C., Suyker, A., Tenhunen, J., Tu, K., Verma, S., Vesala, T., Wilson, K., and Wofsy, S.: Gap filling strategies for defensible annual sums of net ecosystem exchange, Agric For Meteorol, 107, 43–69, https://doi.org/10.1016/S0168-1923(00)00225-2, 2001.

Heiskanen, J., Brümmer, C., Buchmann, N., Calfapietra, C., Chen, H., Gielen, B., Gkritzalis, T., Hammer, S., Hartman, S., Herbst, M., Janssens, I. A., Jordan, A., Juurola, E., Karstens, U., Kasurinen, V., Kruijt, B., Lankreijer, H., Levin, I., Linderson, M.-L., Loustau, D., Merbold, L., Myhre, C. L., Papale, D., Pavelka, M., Pilegaard, K., Ramonet, M., Rebmann, C., Rinne, J., Rivier, L., Saltikoff, E., Sanders, R., Steinbacher, M., Steinhoff, T., Watson, A., Vermeulen, A. T., Vesala, T., Vítková, G., and Kutsch, W.: The Integrated Carbon Observation System in Europe, Bull Am Meteorol Soc, 103, E855–E872, https://doi.org/10.1175/BAMS-D-19-0364.1, 2022.

Hommeltenberg, J., Schmid, H. P., Drösler, M., and Werle, P.: Can a bog drained for forestry be a stronger carbon sink than a natural bog forest?, Biogeosciences, 11, 3477–3493, https://doi.org/10.5194/bg-11-3477-2014, 2014.

ICOS Sweden: Collection of Abisko Stordalen Palsa Bog Swedish network data, https://doi.org/10.18160/Q6H6-B94B, 2023.

Jackowicz-Korczyński, M., Christensen, T. R., Bäckstrand, K., Crill, P., Friborg, T., Mastepanov, M., and Ström, L.: Annual cycle of methane emission from a subarctic peatland, J Geophys Res Biogeosci, 115, https://doi.org/10.1029/2008JG000913, 2010.

Jammet, M., Crill, P., Dengel, S., and Friborg, T.: Large methane emissions from a subarctic lake during spring thaw: Mechanisms and landscape significance, J Geophys Res Biogeosci, 120, 2289–2305, https://doi.org/10.1002/2015JG003137, 2015.

Jammet, M., Dengel, S., Kettner, E., Parmentier, F.-J. W., Wik, M., Crill, P., and Friborg, T.: Year-round CH4 and CO2 flux dynamics in two contrasting freshwater ecosystems of the subarctic, Biogeosciences, 14, 5189–5216, https://doi.org/10.5194/bg-14-5189-2017, 2017.

Jansen, J., Thornton, B. F., Jammet, M. M., Wik, M., Cortés, A., Friborg, T., MacIntyre, S., and Crill, P. M.: Climate-Sensitive Controls on Large Spring Emissions of CH4 and CO2 From Northern Lakes, J Geophys Res Biogeosci, 124, 2379–2399, https://doi.org/10.1029/2019JG005094, 2019.

Johansson, M., Callaghan, T. v., Bosiö, J., Åkerman, H. J., Jackowicz-Korczynski, M., and Christensen, T. R.: Rapid responses of permafrost and vegetation to experimentally increased snow cover in sub-arctic Sweden, Environmental Research Letters, 8, https://doi.org/10.1088/1748-9326/8/3/035025, 2013.

Johansson, T., Malmer, N., Crill, P. M., Friborg, T., Åkerman, J. H., Mastepanov, M., and Christensen, T. R.: Decadal vegetation changes in a northern peatland, greenhouse gas fluxes and net radiative forcing, Glob Chang Biol, 12, 2352–2369, https://doi.org/10.1111/j.1365-2486.2006.01267.x, 2006.

Knox, S. H., Matthes, J. H., Sturtevant, C., Oikawa, P. Y., Verfaillie, J., and Baldocchi, D.: Biophysical controls on interannual variability in ecosystem-scale CO2 and CH4 exchange in a California rice paddy, J Geophys Res Biogeosci, 121, 978–1001, https://doi.org/10.1002/2015JG003247, 2016.

Koven, C. D., Chambers, J. Q., Georgiou, K., Knox, R., Negron-Juarez, R., Riley, W. J., Arora, V. K., Brovkin, V., Friedlingstein, P., and Jones, C. D.: Controls on terrestrial carbon feedbacks by productivity versus turnover in the CMIP5 Earth System Models, Biogeosciences, 12, 5211–5228, https://doi.org/10.5194/bg-12-5211-2015, 2015.

Kuhn, M. A., Thompson, L. M., Winder, J. C., Braga, L. P. P., Tanentzap, A. J., Bastviken, D., and Olefeldt, D.: Opposing Effects of Climate and Permafrost Thaw on CH4 and CO2 Emissions From Northern Lakes, AGU Advances, 2, https://doi.org/10.1029/2021av000515, 2021.

Kutzbach, L., Schneider, J., Sachs, T., Giebels, M., Nykänen, H., Shurpali, N. J., Martikainen, P. J., Alm, J., and Wilmking, M.: CO2 flux determination by closed-chamber methods can be seriously biased by inappropriate application of linear regression, Biogeosciences, 4, 1005–1025, https://doi.org/10.5194/bg-4-1005-2007, 2007.

https://doi.org/10.5194/egusphere-2026-5405
Preprint. Discussion started: 21 September 2026

Łakomiec, P., Holst, J., Friborg, T., Crill, P., Rakos, N., Kljun, N., Olsson, P.-O., Eklundh, L., Persson, A., and Rinne, J.: Field-scale CH4 emission at a subarctic mire with heterogeneous permafrost thaw status, Biogeosciences, 18, 5811–5830, https://doi.org/10.5194/bg-18-5811-2021, 2021.

Lasslop, G., Reichstein, M., Papale, D., Richardson, A. D., Arneth, A., Barr, A., Stoy, P., and Wohlfahrt, G.: Separation of net ecosystem exchange into assimilation and respiration using a light response curve approach: critical issues and global evaluation, Glob Chang Biol, 16, 187–208, https://doi.org/10.1111/j.1365-2486.2009.02041.x, 2010.

Levenberg, K.: A method for the solution of certain non-linear problems in least squares, Q. Appl. Math., 2, 164–168, 1944

Li, T., Raivonen, M., Alekseychik, P., Aurela, M., Lohila, A., Zheng, X., Zhang, Q., Wang, G., Mammarella, I., Rinne, J., Yu, L., Xie, B., Vesala, T., and Zhang, W.: Importance of vegetation classes in modeling CH4 emissions from boreal and subarctic wetlands in Finland, Science of The Total Environment, 572, 1111–1122, https://doi.org/10.1016/j.scitotenv.2016.08.020, 2016.

Liu, L., Schaefer, K., Zhang, T., and Wahr, J.: Estimating 1992–2000 average active layer thickness on the Alaskan North Slope from remotely sensed surface subsidence, J Geophys Res Earth Surf, 117, https://doi.org/10.1029/2011JF002041, 2012.

López-Blanco, E., Langen, P. L., Williams, M., Christensen, J. H., Boberg, F., Langley, K., and Christensen, T. R.: The future of tundra carbon storage in Greenland – Sensitivity to climate and plant trait changes, Science of The Total Environment, 846, 157385, https://doi.org/10.1016/j.scitotenv.2022.157385, 2022.

Lundin, E. J., Klaminder, J., Giesler, R., Persson, A., Olefeldt, D., Heliasz, M., Christensen, T. R., and Karlsson, J.: Is the subarctic landscape still a carbon sink? Evidence from a detailed catchment balance, Geophys Res Lett, 43, 1988–1995, https://doi.org/10.1002/2015GL066970, 2016.

MacDougall, A. H. and Knutti, R.: Projecting the release of carbon from permafrost soils using a perturbed parameter ensemble modelling approach, Biogeosciences, 13, 2123–2136, https://doi.org/10.5194/bg-13-2123-2016, 2016.

Malmer, N., Johansson, T., Olsrud, M., and Christensen, T. R.: Vegetation, climatic changes and net carbon sequestration in a North-Scandinavian subarctic mire over 30 years, Glob Chang Biol, 11, 1895–1909, https://doi.org/10.1111/j.1365-2486.2005.01042.x, 2005.

Marquardt, D. W.: An Algorithm for Least-Squares Estimation of Nonlinear Parameters, Journal of the Society for Industrial and Applied Mathematics, 11, 431–441, 1963.

McGuire, A. D., Lawrence, D. M., Koven, C., Clein, J. S., Burke, E., Chen, G., Jafarov, E., MacDougall, A. H., Marchenko, S., Nicolsky, D., Peng, S., Rinke, A., Ciais, P., Gouttevin, I., Hayes, D. J., Ji, D., Krinner, G., Moore, J. C., Romanovsky, V., Schädel, C., Schaefer, K., Schuur, E. A. G., and Zhuang, Q.: Dependence of the evolution of carbon dynamics in the northern permafrost region on the

https://doi.org/10.5194/egusphere-2026-5405
Preprint. Discussion started: 21 September 2026

trajectory of climate change, Proceedings of the National Academy of Sciences, 115, 3882–3887, https://doi.org/10.1073/pnas.1719903115, 2018.

Natali, S. M., Watts, J. D., Rogers, B. M., Potter, S., Ludwig, S. M., Selbmann, A.-K., Sullivan, P. F., Abbott, B. W., Arndt, K. A., Birch, L., Björkman, M. P., Bloom, A. A., Celis, G., Christensen, T. R., Christiansen, C. T., Commane, R., Cooper, E. J., Crill, P., Czimczik, C., Davydov, S., Du, J., Egan, J. E., Elberling, B., Euskirchen, E. S., Friborg, T., Genet, H., Göckede, M., Goodrich, J. P., Grogan, P., Helbig, M., Jafarov, E. E., Jastrow, J. D., Kalhori, A. A. M., Kim, Y., Kimball, J. S., Kutzbach, L., Lara, M. J., Larsen, K. S., Lee, B.-Y., Liu, Z., Loranty, M. M., Lund, M., Lupascu, M., Madani, N., Malhotra, A., Matamala, R., McFarland, J., McGuire, A. D., Michelsen, A., Minions, C., Oechel, W. C., Olefeldt, D., Parmentier, F.-J. W., Pirk, N., Poulter, B., Quinton, W., Rezanezhad, F., Risk, D., Sachs, T., Schaefer, K., Schmidt, N. M., Schuur, E. A. G., Semenchuk, P. R., Shaver, G., Sonnentag, O., Starr, G., Treat, C. C., Waldrop, M. P., Wang, Y., Welker, J., Wille, C., Xu, X., Zhang, Z., Zhuang, Q., and Zona, D.: Large loss of CO2 in winter observed across the northern permafrost region, Nat Clim Chang, 9, 852–857, https://doi.org/10.1038/s41558-019-0592-8, 2019.

Palace, M., Herrick, C., DelGreco, J., Finnell, D., Garnello, A. J., McCalley, C., McArthur, K., Sullivan, F., and Varner, R. K.: Determining subarctic peatland vegetation using an unmanned aerial system (UAS), Remote Sens (Basel), 10, https://doi.org/10.3390/rs10091498, 2018.

Peters, W., Bastos, A., Ciais, P., and Vermeulen, A.: A historical, geographical and ecological perspective on the 2018 European summer drought, Philosophical Transactions of the Royal Society B: Biological Sciences, 375, 20190505, https://doi.org/10.1098/rstb.2019.0505, 2020.

Petrescu, A. M. R., Lohila, A., Tuovinen, J.-P., Baldocchi, D. D., Desai, A. R., Roulet, N. T., Vesala, T., Dolman, A. J., Oechel, W. C., Marcolla, B., Friborg, T., Rinne, J., Matthes, J. H., Merbold, L., Meijide, A., Kiely, G., Sottocornola, M., Sachs, T., Zona, D., Varlagin, A., Lai, D. Y. F., Veenendaal, E., Parmentier, F.-J. W., Skiba, U., Lund, M., Hensen, A., van Huissteden, J., Flanagan, L. B., Shurpali, N. J., Grünwald, T., Humphreys, E. R., Jackowicz-Korczyński, M., Aurela, M. A., Laurila, T., Grüning, C., Corradi, C. A. R., Schrier-Uijl, A. P., Christensen, T. R., Tamstorf, M. P., Mastepanov, M., Martikainen, P. J., Verma, S. B., Bernhofer, C., and Cescatti, A.: The uncertain climate footprint of wetlands under human pressure, Proceedings of the National Academy of Sciences, 112, 4594–4599, https://doi.org/10.1073/pnas.1416267112, 2015.

Post, E., Alley, R. B., Christensen, T. R., Macias-Fauria, M., Forbes, B. C., Gooseff, M. N., Iler, A., Kerby, J. T., Laidre, K. L., Mann, M. E., Olofsson, J., Stroeve, J. C., Ulmer, F., Virginia, R. A., and Wang, M.: The polar regions in a 2°C warmer world, Sci Adv, 5, https://doi.org/10.1126/sciadv.aaw9883, 2019.

Pugh, T. A. M., Jones, C. D., Huntingford, C., Burton, C., Arneth, A., Brovkin, V., Ciais, P., Lomas, M., Robertson, E., Piao, S. L., and Sitch, S.: A Large Committed Long-Term Sink of Carbon due to Vegetation Dynamics, Earths Future, 6, 1413–1432, https://doi.org/10.1029/2018EF000935, 2018.

Rafat, A., Byun, E., Rezanezhad, F., Quinton, W. L., Humphreys, E. R., Webster, K., and van Cappellen, P.: The definition of the non-growing season matters: a case study of net ecosystem carbon exchange from a Canadian peatland, Environ Res Commun, 4, 021003, https://doi.org/10.1088/2515-7620/ac53c2, 2022.

Ramage, J., Kuhn, M., Virkkala, A. M., Voigt, C., Marushchak, M. E., Bastos, A., Biasi, C., Canadell, J. G., Ciais, P., López-Blanco, E., Natali, S. M., Olefeldt, D., Potter, S., Poulter, B., Rogers, B. M., Schuur, E. A. G., Treat, C., Turetsky, M. R., Watts, J., and Hugelius, G.: The Net GHG Balance and Budget of the Permafrost Region (2000–2020) From Ecosystem Flux Upscaling, Global Biogeochem Cycles, 38, https://doi.org/10.1029/2023GB007953, 2024.

Rebmann, C., Aubinet, M., Schmid, H., Arriga, N., Aurela, M., Burba, G., Clement, R., de Ligne, A., Fratini, G., Gielen, B., Grace, J., Graf, A., Gross, P., Haapanala, S., Herbst, M., Hörtnagl, L., Ibrom, A., Joly, L., Kljun, N., Kolle, O., Kowalski, A., Lindroth, A., Loustau, D., Mammarella, I., Mauder, M., Merbold, L., Metzger, S., Mölder, M., Montagnani, L., Papale, D., Pavelka, M., Peichl, M., Roland, M., Serrano-Ortiz, P., Siebicke, L., Steinbrecher, R., Tuovinen, J.-P., Vesala, T., Wohlfahrt, G., and Franz, D.: ICOS eddy covariance flux-station site setup: a review, Int Agrophys, 32, 471–494, https://doi.org/10.1515/intag-2017-0044, 2018.

Reichstein, M., Kätterer, T., Andrén, O., Ciais, P., Schulze, E.-D., Cramer, W., Papale, D., and Valentini, R.: Temperature sensitivity of decomposition in relation to soil organic matter pools: critique and outlook, Biogeosciences, 2, 317–321, https://doi.org/10.5194/bg-2-317-2005, 2005.

Rinne, J., Tuittila, E., Peltola, O., Li, X., Raivonen, M., Alekseychik, P., Haapanala, S., Pihlatie, M., Aurela, M., Mammarella, I., and Vesala, T.: Temporal Variation of Ecosystem Scale Methane Emission From a Boreal Fen in Relation to Temperature, Water Table Position, and Carbon Dioxide Fluxes, Global Biogeochem Cycles, 32, 1087–1106, https://doi.org/10.1029/2017GB005747, 2018.

Rinne, J., Tuovinen, J.-P., Klemedtsson, L., Aurela, M., Holst, J., Lohila, A., Weslien, P., Vestin, P., Łakomiec, P., Peichl, M., Tuittila, E.-S., Heiskanen, L., Laurila, T., Li, X., Alekseychik, P., Mammarella, I., Ström, L., Crill, P., and Nilsson, M. B.: Effect of the 2018 European drought on methane and carbon dioxide exchange of northern mire ecosystems, Philosophical Transactions of the Royal Society B: Biological Sciences, 375, 20190517, https://doi.org/10.1098/rstb.2019.0517, 2020.

Rouse Jr., J. W., Haas, R. H., Deering, D. W., and Schell, J. A.: Monitoring the vernal advancement and retrogradation (green wave effect) of natural vegetation, NASA Contractor Report, NASA-CR-136103, NASA, 1973.

Runkle, B. R. K., Sachs, T., Wille, C., Pfeiffer, E.-M., and Kutzbach, L.: Bulk partitioning the growing season net ecosystem exchange of CO2 in Siberian tundra reveals the seasonality of its carbon sequestration strength, Biogeosciences, 10, 1337–1349, https://doi.org/10.5194/bg-10-1337-2013, 2013.

Running, S. W., Baldocchi, D. D., Turner, D. P., Gower, S. T., Bakwin, P. S., and Hibbard, K. A.: A Global Terrestrial Monitoring Network Integrating Tower Fluxes, Flask Sampling, Ecosystem Modeling and EOS Satellite Data, Remote Sens Environ, 70, 108–127, https://doi.org/10.1016/S0034-4257(99)00061-9, 1999.

Schuur, E. A. G. and Mack, M. C.: Ecological Response to Permafrost Thaw and Consequences for Local and Global Ecosystem Services, Annu Rev Ecol Evol Syst, 49, 279–301, https://doi.org/10.1146/annurev-ecolsys-121415-032349, 2018.

Schuur, E. A. G., Bockheim, J., Canadell, J. G., Euskirchen, E., Field, C. B., Goryachkin, S. v., Hagemann, S., Kuhry, P., Lafleur, P. M., Lee, H., Mazhitova, G., Nelson, F. E., Rinke, A., Romanovsky, V. E., Shiklomanov, N., Tarnocai, C., Venevsky, S., Vogel, J. G., and Zimov, S. A.: Vulnerability of Permafrost Carbon to Climate Change: Implications for the Global Carbon Cycle, Bioscience, 58, 701–714, https://doi.org/10.1641/B580807, 2008.

Serreze, M. C., Barrett, A. P., and Cassano, J. J.: Circulation and surface controls on the lower tropospheric air temperature field of the Arctic, Journal of Geophysical Research Atmospheres, 116, https://doi.org/10.1029/2010JD015127, 2011.

Taillardat, P., Bodmer, P., Deblois, C. P., Ponçot, A., Prijac, A., Riahi, K., Gandois, L., del Giorgio, P. A., Bourgault, M. A., Tremblay, A., and Garneau, M.: Carbon Dioxide and Methane Dynamics in a Peatland Headwater Stream: Origins, Processes and Implications, J Geophys Res Biogeosci, 127, https://doi.org/10.1029/2022JG006855, 2022.

Treat, C. C., Marushchak, M. E., Voigt, C., Zhang, Y., Tan, Z., Zhuang, Q., Virtanen, T. A., Räsänen, A., Biasi, C., Hugelius, G., Kaverin, D., Miller, P. A., Stendel, M., Romanovsky, V., Rivkin, F., Martikainen, P. J., and Shurpali, N. J.: Tundra landscape heterogeneity, not interannual variability, controls the decadal regional carbon balance in the Western Russian Arctic, Glob Chang Biol, 24, 5188–5204, https://doi.org/10.1111/gcb.14421, 2018.

Varner, R. K., Crill, P. M., Frolking, S., McCalley, C. K., Burke, S. A., Chanton, J. P., Holmes, M. E., Saleska, S., and Palace, M. W.: Permafrost thaw driven changes in hydrology and vegetation cover increase trace gas emissions and climate forcing in Stordalen Mire from 1970 to 2014, Philosophical Transactions of the Royal Society A: Mathematical, Physical and Engineering Sciences, 380, https://doi.org/10.1098/rsta.2021.0022, 2022.

Varney, R. M., Chadburn, S. E., Friedlingstein, P., Burke, E. J., Koven, C. D., Hugelius, G., and Cox, P. M.: A spatial emergent constraint on the sensitivity of soil carbon turnover to global warming, Nat Commun, 11, https://doi.org/10.1038/s41467-020-19208-8, 2020.

Voigt, C., Marushchak, M. E., Abbott, B. W., Biasi, C., Elberling, B., Siciliano, S. D., Sonnentag, O., Stewart, K. J., Yang, Y., and Martikainen, P. J.: Nitrous oxide emissions from permafrost-affected soils, Nat Rev Earth Environ, 1, 420–434, https://doi.org/10.1038/s43017-020-0063-9, 2020.

https://doi.org/10.5194/egusphere-2026-5405
Preprint. Discussion started: 21 September 2026

Walczak, S. and Cerpa, N.: Artificial Neural Networks, in: Encyclopedia of Physical Science and Technology, Elsevier, 631–645, https://doi.org/10.1016/B0-12-227410-5/00837-1, 2003.

Watts, J. D., Farina, M., Kimball, J. S., Schiferl, L. D., Liu, Z., Arndt, K. A., Zona, D., Ballantyne, A., Euskirchen, E. S., Parmentier, F. W., Helbig, M., Sonnentag, O., Tagesson, T., Rinne, J., Ikawa, H., Ueyama, M., Kobayashi, H., Sachs, T., Nadeau, D. F., Kochendorfer, J., Jackowicz-Korczynski, M., Virkkala, A., Aurela, M., Commane, R., Byrne, B., Birch, L., Johnson, M. S., Madani, N., Rogers, B., Du, J., Endsley, A., Savage, K., Poulter, B., Zhang, Z., Bruhwiler, L. M., Miller, C. E., Goetz, S., and Oechel, W. C.: Carbon uptake in Eurasian boreal forests dominates the high-latitude net ecosystem carbon budget, Glob Chang Biol, 29, 1870–1889, https://doi.org/10.1111/gcb.16553, 2023.

Wilson, R. M., Hough, M. A., Verbeke, B. A., Hodgkins, S. B., Chanton, J. P., Saleska, S. D., Rich, V. I., Tfaily, M. M., Tyson, G., Sullivan, M. B., Brodie, E., Riley, W. J., Woodcroft, B., McCalley, C., Dominguez, S. C., Crill, P. M., Varner, R. K., Frolking, S., and Cooper, W. T.: Plant organic matter inputs exert a strong control on soil organic matter decomposition in a thawing permafrost peatland, Science of The Total Environment, 820, 152757, https://doi.org/10.1016/j.scitotenv.2021.152757, 2022.

Wu, Y., Mao, X., Zhang, Z., Tang, W., Cao, G., Zhou, H., Ma, J., and Yin, X.: Temporal and spatial characteristics of CO2 flux in plateau urban wetlands and their influencing factors based on Eddy covariance technique, Water (Switzerland), 13, https://doi.org/10.3390/w13091176, 2021.

Wutzler, T., Lucas-Moffat, A., Migliavacca, M., Knauer, J., Sickel, K., Šigut, L., Menzer, O., and Reichstein, M.: Basic and extensible post-processing of eddy covariance flux data with REddyProc, Biogeosciences, 15, 5015–5030, https://doi.org/10.5194/bg-15-5015-2018, 2018.

Yu, Z., Loisel, J., Brosseau, D. P., Beilman, D. W., and Hunt, S. J.: Global peatland dynamics since the Last Glacial Maximum, Geophys Res Lett, 37, https://doi.org/10.1029/2010GL043584, 2010.

Yurova, A., Wolf, A., Sagerfors, J., and Nilsson, M.: Variations in net ecosystem exchange of carbon dioxide in a boreal mire: Modeling mechanisms linked to water table position, J Geophys Res Biogeosci, 112, https://doi.org/10.1029/2006JG000342, 2007.